Tarapacá intermediate-depth earthquake (Mw 7.7, 2005, northern Chile): A slab-pull event with horizontal fault plane constrained from seismologic and geodetic observations

S Peyrat, J Campos, Jean-Bernard de Chabalier, S Bonvalot, M.-P Bouin, D Legrand, A Nercessian, Olivier Charade, G Patau, E Clévédé, et al.

Tarapacá intermediate-depth earthquake (Mw 7.7, 2005, northern Chile): A slab-pull event with horizontal fault plane constrained from seismologic and geodetic observations

S. Peyrat,[1] J. Campos,[2] J. B. de Chabalier,[3] A. Perez,[2] S. Bonvalot,[2,4] M.-P. Bouin,[1] D. Legrand,[2] A. Nercessian,[3] O. Charade,[1] G. Patau,[1] E. Clévédé,[1] E. Kausel,[2] P. Bernard,[1] and J.-P. Vilotte[1]

Received 1 August 2006; revised 11 October 2006; accepted 18 October 2006; published 28 November 2006.

[1] A large (Mw 7.7) intermediate-depth earthquake occurred on 13 June 2005 in the Tarapacá region of the northern Chile seismic gap. Source parameters are inferred from teleseismic broadbands, strong motions, GPS and InSAR data. Relocated hypocenter is found at ~98 km depth within the subducting slab. The 21-days aftershock distribution, constrained by a postseismic temporary array, indicates a sub-horizontal fault plane lying between the planes of the double seismic zone and an upper bound of the rupture area of 60 km × 30 km. Teleseismic inversion shows a slab-pull down dip extension mechanism on a nearly horizontal plane. Total seismic and geodetic moments are $\sim 5.5 \times 10^{20}$ N.m, with an averaged slip of 6.5 m from geodesy. The earthquake rupture is peculiar in that the effective velocity is slow, 3.5 Km.s^{-1} for a high stress-drop, 21–30 MPa. We propose that rupture was due to the reactivation by hydraulic embrittlement of a inherited major lithospheric fault within the subducting plate. The stress-drop suggests that the region of the slab between planes of the double seismic zone can sustain high stresses.
Citation: Peyrat, S., et al. (2006), Tarapacá intermediate-depth earthquake (Mw 7.7, 2005, northern Chile): A slab-pull event with horizontal fault plane constrained from seismologic and geodetic observations, *Geophys. Res. Lett.*, *33*, L22308, doi:10.1029/2006GL027710.

1. Introduction

[2] The 13 June 2005 at T.O. 22:44:30 (UTC), an intermediate-depth intraplate earthquake (Mw 7.7) occurred in the Tarapacá region of northern Chile, below the French-Chilean permanent GPS network. This is one of the largest inland earthquakes in northern Chile since the 1950 Antofagasta earthquake (Ms = 8, 9 December 1950). In that region the Nazca plate dips at approximatively 20°–30° beneath the South American plate and exhibits a complex three-dimensional structure [*Comte et al.*, 1994; *Rietbrock and Haberland*, 2001]. Following the earthquake a temporary seismic array was rapidly deployed during a coordinated postseismic intervention. In North Chile, between Arica (18°S) and Antofagasta (23.5°S), the last megathrust earthquake dates back to the 1877 Iquique (Mw ~ 9.0, 10 May 1877) earthquakes that produced destructive Pacific-wide tsunami [*Comte and Pardo*, 1991; *Kausel and Campos*, 1992]. The northern and southern segments have been ruptured respectively by the Antofagasta (Mw = 8.1, 30 July 1995) and the Arequipa (Mw = 8.3, 23 June 2001) earthquakes [e.g. *Ruegg et al.*, 1996, 2001; *Chlieh et al.*, 2004]. Others intermediate-depth earthquakes are reported in northern Chile [*Delouis et al.*, 1996; *Araujo and Suárez*, 1994; *Kausel and Campos*, 1992], with predominantly down-dip tensional axes, and have been sometimes associated [*Aztiz et al.*, 1988] to variation of interplate coupling during the earthquake cycle. The Tarapacá earthquake is reminiscent of the 1950 Antofagasta down-dip tensional intraplate earthquake.

[3] Intermediate-depths seismicity in northern Chile delineates a double seismic zone [*Rietbrock and Waldhauser*, 2004; *Comte and Suárez*, 1994], although detailed resolution remains limited by the uncertainties of the hypocenter depth locations. At intermediate depths, earthquakes are thought to be enabled by dehydration of hydrous minerals [*Kirby*, 1995; *Peacock*, 2001; *Jung et al.*, 2004]. The mechanism by which dehydration triggers earthquakes remains poorly understood but radiation patterns of intermediate-depth events suggest shear dislocation as a primary mechanism. In the case of a double seismic zone, the existence of a lower layer of seismicity raises the question of the presence of hydrous phases into the mantle of the slab or another mechanism triggers earthquakes here [*Kirby et al.*, 1996]. In Japan, large intermediate-depth earthquakes have also been reported to indicate fault planes lying horizontally between the double seismic zone, e.g. the 1993 Mw 7.9 Kushiro-oki earthquake [*Ide and Takeo*, 1996].

2. Mainshock and Aftershocks

[4] One week after the mainshock, a temporary seismic network of eight short-periods (4.5 Hz and 1 Hz sensors; 20-bit and 16-bit continuous recording at 50 Hz) and four broadband instruments (1 CMG-40 and 3 STS-2, 24-bit continuous recording at 50 Hz and 40 Hz), was deployed during a postseismic intervention within the focal area (see

[1]Seismology Laboratory, UMR 7154, CNRS, Institut de Physique du Globe de Paris, Paris, France.
[2]Departamento de Geofísica, Universidad de Chile, Santiago, Chile.
[3]Geodesy Laboratory, UMR 7154, CNRS, Institute de Physique du Globe de Paris, Paris, France.
[4]Laboratoire des Mécanismes et Transferts Géologique, UMR 5563, Institut de Recherche pour le Développement, UR154, CNRS, Toulouse, France.

0094-8276/06/2006GL027710

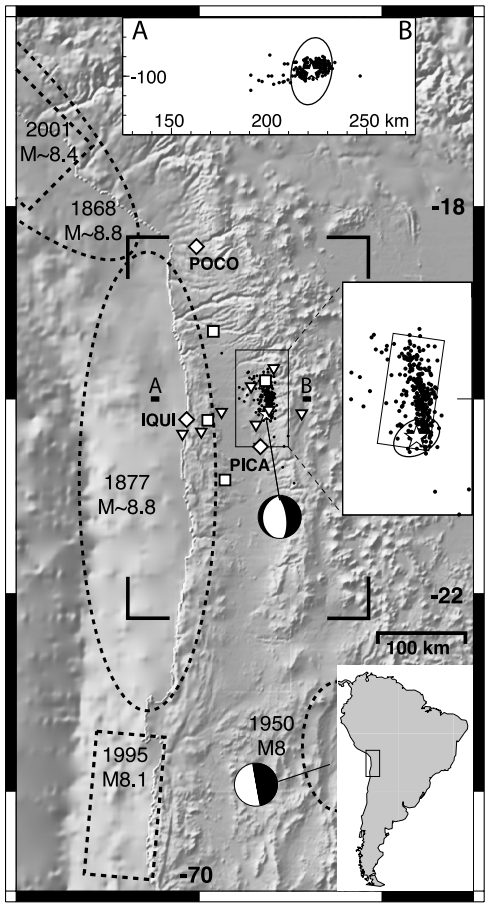

Figure 1. Rupture areas of the last large earthquakes in northern Chile, location of the mainshock and distribution of the aftershocks of the 13 June 2005 Tarapacá earthquake. White symbols show the locations of seismological stations, diamonds indicate accelerometers, squares indicate broadbands, and inverse triangles indicate short periods. The relocated hypocenter with error ellipse is shown as a white star and the 21 days selected aftershocks as filled black circles. (inset right) Enlargement of the epicenter area with the fault area of the geodetic study. (inset above) E-W cross section of aftershocks relative to the trench. The 1950 Antofagasta and 2005 Tarapacá focal mechanisms are also reported. The four corners indicate the map coverage of Figure 3.

Figure 1 and Table S1[1]). Aftershocks sequence used here spans between 20 June and 5 July 2005. All stations were used. The 317 best located events were selected (with at least 5 stations and 5 S-phases, rms $\leq$ 0.2). The magnitude threshold is estimated at Mw 2.5, and the largest recorded one is ~Mw 5. Aftershocks locations are determined with the probabilistic hypocentral location algorithm of *Lomax et al.* [2001], NonLinLoc software, using arrival times and a non linear grid-search algorithm allowing an estimate of the a-posteriori probability density function (PDF) and of the maximum hypocenter likelihood. Based on the work by *ANCORP Working Group* [2003], the velocity model in Table 1 has been used. The maximum likelihood of the aftershocks hypocenter locations are shown Figure 1, with an averaged hypocentral uncertainties of ~5 km in all directions and a rms of ~0.2. The aftershocks distribution is confined within a subhorizontal tabular area of about 60 km length and 30 km width, elongated in the north-south direction and slightly dipping to the west, identified as the fault plane (Table S2).

[5] To improve the mainshock hypocenter determination, a relative location is performed, using a master event technique, with respect to a well located large aftershock. The permanent network of strong-motions (EpiSensor, 2g full scale range, 24-bit digital signal), operated in triggered mode by the University of Chile (http://www.cec.uchile.cl/~ragic/ragic.htm), recorded both the mainshock and the main aftershocks at local and regional distances. However, only the largest aftershock of the sequence (14 August 2005, Mw = 5.9, NEIC) was recorded by three stations of the network (IQUI, PICA and POCO, see Figure 1). It occurred when part of the temporary network was already removed and its location is not very accurate. A two steps procedure is therefore considered: first, using an aftershock (02 July 2005, Mb = 4.2, NEIC) well located by the temporary network and recorded on 2 strong-motion stations (PICA and IQUI), the 14 August aftershock is relocated; second, using this relocated aftershock, the mainshock is relocated. For the mainshock relocation, the inferred non-linear PDF exhibits a single maximum and an ellipsoidal shape. The confidence ellipsoid parameters are for the azimuth, dip and length of the semi-axis of axis 1 (174.9°, −27.5°, 4.8 km) and for axis 2 (90.1°, 9.8°, 1.1 km), while the semi-axis of axis 3 is 2.1 km, and provide a good indicator of the uncertainties. We report in Figure 1 the maximum likelihood of the relocated mainshock hypocenter (Latitude, −20.168°; Longitude, −69.264°; depth, 97.6 km) together with the 68% confidence ellipsoid.

[6] A centroid moment tensor (CMT) solution was determined using long period surface waves recorded at stations of Geoscope and IRIS networks. The solution is reported in Table 2, referred as Geoscope solution, together with solutions from other agencies. The CMT solution shows a downdip extension mechanism, with a low dip nodal-plane consistent with the aftershock distribution. Consequently, the fault plane of the Tarapacá earthquake is assumed to be sub-horizontal.

3. Far-Field Body Wave Analysis

[7] Thirty VBB stations of the IRIS and Geoscope networks have been used for wave-form modeling. Only stations at epicentral distances between 30° and 90° for

Table 1. Velocity Model

P-velocity, km/s	Depth, km
4.8	0.
6.2	10.
6.7	20.
7.3	50.
7.7	60.
8.1	80.

[1]Auxiliary material data sets are available at ftp://ftp.agu.org/apend/gl/2006gl027710. Other auxiliary material files are in the HTML.

Table 2. CMT Solutions

	Lat., deg.	Long., deg.	Depth, km	Strike	Dip, deg.	Slip, deg.	Mo., 10^{20} Nm
Geoscope[a]	−20.	−69.2	95.	192.	29.	−72.	4.54
Harvard	−20.02	−69.17	95.3	182.	24.	−81.	5.1
USGS	−19.90	−69.13	101.	231.	30.	−33.	6.5

[a]This study.

the P-waves, and between 34° and 87° for SH-waves, are retained to avoid multipathing, upper mantle and core arrivals. Source parameters are determined using the inversion method of *Nábělek* [1984], assuming a double-couple point source. At the source, the velocity structure of Table 1 is considered, while a homogeneous half-space is assumed at the receivers, e.g. V_p = 6.4 km/s, V_s = 3.7 km/s, ρ = 2.8 gr/cm^3. The displacements data are band-passed filtered, by a 3 poles Butterworth filter (0.01 Hz–1.0 Hz), to avoid the small scale structures. In a first step, a source depth is inferred, by simple trial and error, at 99 km in good agreement with the hypocenter depth determined from strong motion data. Fixing that depth, the focal mechanism and the source time function are inverted simultaneously from body waveforms using our CMT solution as an a-priori model. The best inferred solution shows a down-dip extension mechanism with dips of 20°/71°, strikes of 189°/352° and rakes of −74°/−96°. Based on the aftershocks distribution analysis, the lower dip nodal-plane is again identified as the fault plane.

[8] The azimuthal distribution of the selected stations well constrains the dip of the auxiliary nodal-plane (Figure 2), but leaves a trade-off between the strike and the rake directions for the low dip-angle plane. A sensitivity analysis is performed to assess a set of admissible models, e.g. models with less than 4% change in waveform residual. When exploring low dip nodal-planes between 18° and 24°, the residual exhibits a broad minimum for strike/rake directions ranging between N172°E and N200°E, pointing out a lack of resolution for these parameters. In Figure 2, the preferred solution, e.g. in terms of compatibility with the geodetic analysis detailed hereafter, is reported. The solution shows a dip angle of 24°, favored by the geodetic analysis, a strike/rake of 189°/−74°. The P and T axes dip at 67°/22° respectively in the 249°/87° directions. For all the admissible models, the inferred P and T axes directions remain very stable despite the strike/rake variations. The total seismic moment is M_0 = 5.4 × 10^{20} N.m. The source time function has a simple shape and a total duration of ∼17s.

4. InSAR and GPS Modeling

[9] Static surface displacement is modeled combining coseismic displacements, from permanent GPS stations, and interferograms from ENVISAT radar images. Data from 7 continuous GPS stations (Table S3) are processed using the GAMIT software [*King and Bock*, 2001], together with igs orbits and tables for modeling the antenna phase center variations. Daily solutions are calculated over 10 day periods prior and after the earthquake, relatively to two distant stations (Mejillones and Arequipa). After averaging, coseismic displacements are defined here as the difference between the resulting mean coordinates prior and after the earthquake. Based on the continuous GPS series, negligible fast post-seismic transients are measured during these time periods, including the day prior and the day after the earthquake (Figure 3 and Figure S1). The estimated combined error in the resulting vectors is less than 2 mm and 4 mm for horizontal and vertical components respectively.

[10] InSAR analysis is performed by processing data that covers most of the deformed area of the Tarapacá earthquake (200 × 200 km), along two adjacent tracks 368 (8 May 2004 and 6 August 2005) and 96 (24 May 2004 and 18 July 2005) from west to east, using the JPL/Caltech ROI_PAC software [*Rosen et al.*, 2004]. The topographic signal is removed from the interferograms using a 3-arc sec SRTM digital elevation model. A significant atmospheric effect (2–5 cm), correlated with the topography, is removed using a linear correlation with the topography. The line of sight component of the earthquake-induced surface displacement is then constructed (Figure 3). The displayed interferograms span time intervals from about 1 year before the earthquake and 1.5 to 1 month after the earthquake, respectively from west to east. The observed interferogram phases contain a small interseismic deformation signal

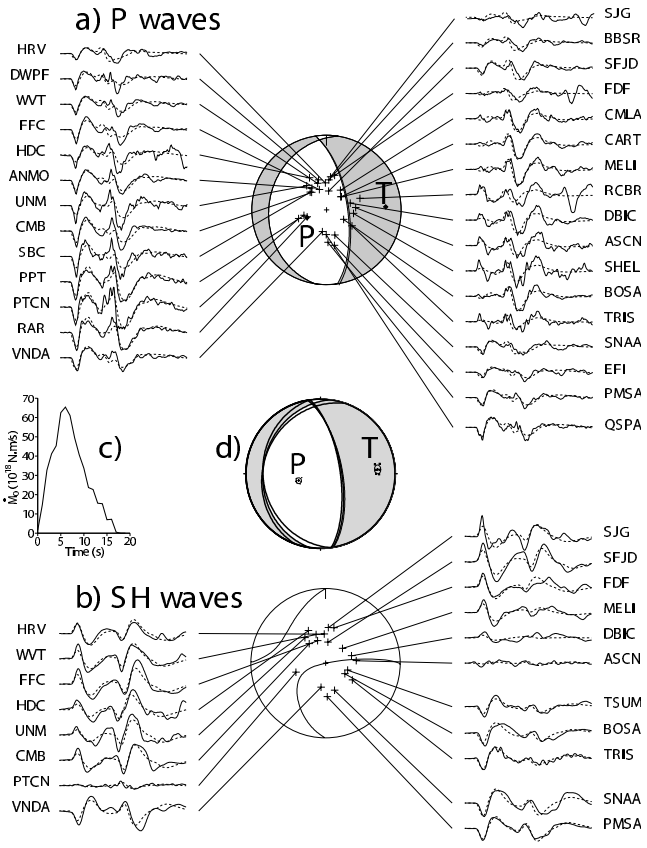

Figure 2. Teleseismic body-wave inversion. Focal mechanism for the preferred solution, e.g. best compatible solution with the geodetic analysis, is shown in observed (solid line) and synthetic (dashed line) for (a) P-displacements waveforms and (b) SH-displacement waveforms, with (c) the time source function. (d) Stability of the maximum (P) and minimum (T) compression axes when exploring low dip planes, as a result of the trade-off between the strike and rake directions.

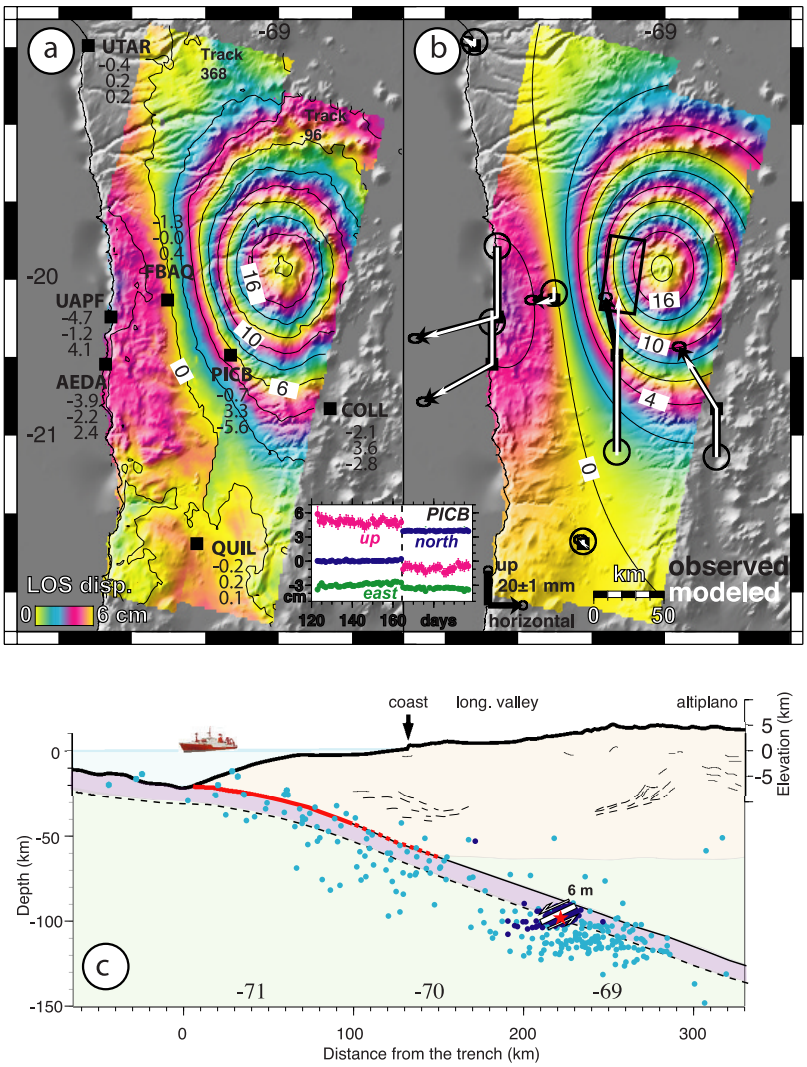

Figure 3. Coseismic surface displacements from (a) ENVISAT acquisition and (b) synthetics using Okada's model. One color cycle represents 6 cm of ground displacement toward the satellite. Coseismic displacements from continuous GPS: Figure 3a observed east, north, up offsets in cm; and Figure 3b observed (black) and modeled (white) with vectors for horizontal components and N-S bars for upward and downward displacements respectively. The inset indicates the 3-component time series of station PICB. (c) Interpretation of the seismological and geodetic fault parameters in a West-East cross section (20°S). Light-blue circles are background seismicity (M > 4.5) from *Engdahl et al.* [1998]. Dark blue circles are the aftershocks. Slab geometry is extrapolated from the ANCORP working group profile at 21°S.

related with megathrust coupling, evidenced by previous study [*Chlieh et al.*, 2004]. To remove most of this signal, as well as the orbital errors, a linear ramp for each track is adjusted. A maximum increase of ∼18 cm in the range displacement is observed slightly east of the epicenter area together with an area of range decrease of ∼2–3 cm along the coast side. This is consistent with a subsidence in the epicentral area and an uplift and a seaward displacements evidenced by continuous GPS.

[11] The coseismic surface displacement field is modeled using a single dislocation, centered at the hypocenter, within a homogeneous elastic half space [*Okada*, 1985]. The dislocation plane is chosen, based on the aftershocks distribution, as a 54 km long × 24 km wide plane dipping to the west. The geodetic model is quite sensitive to the dip angle of the fault plane, especially with regard to the horizontal-to-vertical ratio of the GPS displacements. The geodetic model favors higher dip and lower strike angles than the seismological models. Due to the trade-off in the teleseismic body-wave inversion between strike and rake, the best compromise between geodesy and seismology is found for a dip angle of 24°, and a strike/rake of 189°/−74° (with a fit that is 20% better when increasing the dip angle from 20° to 24°). The total slip is 6.5 m, with a geodetic moment of 5.8×10^{20} N.m assuming an effective shear modulus of 6.5×10^{10} Pa for the geodesy, in good agreement with the seismic moment obtained by body wave inversion. The resulting model is shown in Figure 3.

5. Discussion and Conclusion

[12] Teleseismic inversion of the large intermediate-depth Tarapacá earthquake (Mw = 7.7) indicates a downdip extension mechanism. The T-axis is roughly perpendicular

to the trench direction with a down-dip alignment. The aftershock distribution delineates a clear sub-horizontal NS oriented planar area, of ~60 km length and 30 km width, providing an upper limit for the rupture area and constraining the low dip nodal-plane as the fault plane. This is consistent with the lack of S-waves directivity observed on the teleseismic stations located on the sub-vertical nodal-plane. The hypocenter is located South of the aftershocks distribution at ~97.6 km depth. Using the inferred source time function and rupture area, a rupture velocity of ~3.5 km.s^{-1} (<77% V_s) is estimated. Both geodetic and seismic moments, ~5.5×10^{20} N.m lead to a high stress-drop estimate of ~20–30 MPa. The rupture is peculiar: a slow effective rupture velocity for a high-stress drop, suggesting a non trivial rupture process.

[13] A widely spaced (>20 km) double-layered Wadati-Benioff zone was found [*Comte and Suárez*, 1994] near Iquique (~−21°S latitude) with down-dip tensional events in the upper plane and compressional events in the lower plane. In contrast [*Rietbrock and Waldhauser*, 2004], using high-precision relocations, found a fine-scale narrowly spaced (8–10 km) double-seismic zone south of Iquique (−22°*S*) with predominantly extensional faulting in both seismic layers, and a clear down-dip tensional regime with T-axes oriented in slab-parallel directions. The upper layer is inferred in the oceanic crust just below the top of the slab, and the lower layer in the uppermost subducting oceanic mantle. Extensional events in the oceanic crust are therefore observed regardless of the apparent stress field in the underlying oceanic mantle, suggesting dehydration embrittlement mechanism and reactivation of inherited oceanic faults.

[14] Aftershock distribution, hypocenter location and high-stress drop suggest that the earthquake occurred within the subducting slab between the planes of the double seismic zone, an area which should be the coldest and strong enough to sustain such high stresses. The rupture may have span the whole WBZ with a sharp termination at both ends as suggested by the lack of short term transients in the geodetic data. The sharp termination of the aftershock distribution toward east may be related to the interface between the oceanic crust and the continental mantle. The Tarapacá earthquake raises the possibility of the reactivation of an inherited major sub-horizontal fault within the oceanic lithosphere. Major oceanic faults are believed to stimulate deep penetration of water, leading hydrous alteration and later dehydration embrittlement processes to the required depths of the WBZ lower layer of seismicity [*Jiao et al.*, 2000; *Peacock*, 2001]. The inferred down-dip extension mechanism support extensional stress regime in the region between the double seismic layers as a result of slab-pull forces. While this is consistent with the stress regime inferred by *Rietbrock and Waldhauser* [2004], the results of *Comte and Suárez* [1994] could suggest that the rupture may have propagated through different stress regimes in the upper and lower seismic zone. Further investigations are required to precise the thermo-mechanical interactions between released fluids and inherited fault systems.

[15] **Acknowledgments.** This study would not have been possible without J.-C. Ruegg, A. Cisternas and R. Madariaga. We thank also C. Aranda, N. Allendes, H. Riquelme, J. Vasquez, M. Thielman of the National Seismological Service of the University of Chile; V. Clouard, G. Gabalda, A. Lemoine and M. Olcay for their help. This work was supported by the Chilean ICM project "Millennium Science Nucleus of Seismotectonics and Seismic Hazard", the Fondecyt project 1030800, the ANR-05-CATT-01402 project of the French National Research Agency and the ACI Jeunes Chercheurs "Risque sismique". We acknowledge the support of the European Space Agency (ESA) for programming Envisat satellite (AO-720), and of the CNRS-INSU Mobile Broadband Network. ROI_PAC software was provided by the JPL/Caltech. Thanks to R. Boroschek for the strong motion data.

References

ANCORP Working Group (2003), Seismic imaging of a convergent continental margin and plateau in the central Andes (Andean Continental Research Project 1996 (ANCORP'96)), *J. Geophys. Res.*, *108*(B7), 2328, doi:10.1029/2002JB001771.

Araujo, M., and G. Suárez (1994), Geometry and state of stress of the subducted Nazca plate beneath central Chile and Argentina: Evidence from teleseismic data, *Geophys. J. Int.*, *116*, 283–303.

Aztiz, L., T. Lay, and H. Kanamori (1988), Large intermediate-depth earthquakes and the subduction process, *Phys. Earth Planet. Inter.*, *53*, 80–166.

Chlieh, M., J. de Chabalier, J. Ruegg, R. Armijo, R. Dmowska, J. Campos, and K. Feigl (2004), Crustal deformation and fault slip during the seismic cycle in the north Chile subduction zone, from GPS and InSAR observations, *Geophys. J. Int.*, *158*, 695–711.

Comte, D., and M. Pardo (1991), Reapraisal of great historical earthquakes in the northern Chile and southern Peru seismic gaps, *Nat. Hazards*, *4*, 23–44.

Comte, D., and G. Suárez (1994), An inverted double-seismic zone in Chile: Evidence of phase transformation in the subducted slab, *Science*, *263*, 212–215.

Comte, D., S. Roecker, and G. Suárez (1994), Velocity structure in northern Chile: Evidence of subducted oceanic crust in the Nazca Plate, *Geophys. J. Int.*, *117*, 625–639.

Delouis, B., A. Cisternas, L. Dorbath, L. Rivera, and E. Kausel (1996), The Andean subduction zone between 22 and 25°S (northern Chile): Precise geometry and state of stress, *Tectonophysics*, *259*, 81–100.

Engdahl, E., R. van der Hilst, and R. Buland (1998), Global teleseismic earthquake relocation with improved travel times and procedures for depth determination, *Bull. Seismol. Soc. Am.*, *88*, 722–743.

Ide, S., and M. Takeo (1996), The dynamic rupture process of the 1993 Kushiro-oki earthquake, *J. Geophys. Res.*, *101*, 5661–5675.

Jiao, W., P. Silver, Y. Fei, and C. Prewitt (2000), Do intermediate- and deep focus earthquakes occur on preexisting weak zones? An examination of the Tonga subduction zone, *J. Geophys. Res.*, *105*(B12), 28,125–28,138.

Jung, H., H. Green II, and L. Dobrzhinetskaya (2004), Intermediate-depth earthquake faulting by dehydration embrittlement with negative volume change, *Nature*, *428*, 545–549.

Kausel, E., and J. Campos (1992), The Ms = 8 tensional earthquake of 9 December 1950 northern Chile and its relation to the seismic potential of the region, *Phys. Earth Planet. Inter.*, *72*, 220–235.

King, R., and Y. Bock (2001), Documentation for the GAMIT GPS software analysis, release 10.05, technical report, Scripps Inst. of Oceanogr., Univ. of Calif., San Diego.

Kirby, S. (1995), Interslab earthquakes and phase changes in subducting lithosphere, *Rev. Geophys.*, *33*(S1), 287–298.

Kirby, S., E. Engdahl, and R. Denlinger (1996), Intermediate-depth intraslab earthquakes and arc volcanism as physical expressions of crustal and uppermost mantle metamorphism in subducting slabs (overview), in *Subduction: Top to Bottom*, *Geophys. Monogr. Ser.*, vol. 96, edited by G. B. et al., pp. 195–214, AGU, Washington, D. C.

Lomax, A., A. Zollo, P. Capuano, and J. Virieux (2001), Precise absolute earthquake location under Somma-Vesuvius volcano using a new 3D velocity model, *Geophys. J. Int.*, *146*, 313–331.

Nábělek, J. (1984), Determination of earthquake source parameters from inversion of body waves, Ph.D. thesis, Mass. Inst. of Technol., Cambridge.

Okada, Y. (1985), Surface deformation due to shear and tensile faults in a half-space, *Bull. Seismol. Soc. Am.*, *75*, 1135–1154.

Peacock, S. (2001), Are the lower planes of double seismic zones caused ber serpentine dehydration in subducting oceanic mantle?, *Geology*, *29*, 299–302.

Rietbrock, A., and C. Haberland (2001), A tear in the subducting Nazca slab: Evidence from local earthquake tomography and high precision hypocenters, *Eos Trans. AGU*, *82*(47), Fall Meet. Suppl., Abstract T31A-0822.

Rietbrock, A., and F. Waldhauser (2004), A narrowly spaced double-seismic zone in the subducting Nazca plate, *Geophys. Res. Lett.*, *31*, L10608, doi:10.1029/2004GL019610.

Rosen, P., S. Hensley, G. Peltzer, and M. Simons (2004), Updated repeat orbit interferometry package released, *Eos Trans. AGU*, *85*(5), 47.

Ruegg, J., et al. (1996), The M_w 8.1 Antofagasta (north Chile) earthquake July 30, 1995: First results from teleseismic and geodetic data, *Geophys. Res. Lett.*, *23*, 917–920.

Ruegg, J., M. Olcay, and D. Lazo (2001), Co-, post- and pre (?)-seismic displacements associated with the Mw = 8.4 southern Peru earthquake of 23 June 2001 from continuous GPS measurements, *Seismol. Res. Lett.*, *72*, 673–678.

P. Bernard, M. P. Bouin, O. Charade, E. Clévédé, G. Patau, S. Peyrat, and J.-P. Vilotte, Seismology Laboratory, UMR 7154, CNRS, Institut de Physique du Globe de Paris, 4 Place Jussieu, F-75252 Paris, France. (vilotte@ipgp.jussieu.fr)

S. Bonvalot, UMR 5563, IRD UR154, CNRS, LMTG, 14 avenue Edouard Belin, F-31000 Toulouse, France. (bonvalot@dgf.uchile.cl)

J. Campos, E. Kausel, D. Legrand, and A. Perez, Depto. Geofísica, Univ. de Chile, Blanch Encalada 2085, Santiago, Chile. (jaime@dgf.uchile.cl)

J. B. de Chabalier and A. Nercessian, Geodesy Laboratory, UMR 7154, CNRS, Institut de Physique du Globe de Paris, 4 Place Jussieu, F-75252 Paris, France. (dechabal@ipgp.jussieu.fr)